Net radiative forcing due to changes in regional emissions of tropospheric ozone precursors

Vaishali Naik,[1] Denise Mauzerall,[1,3] Larry Horowitz,[2] M. Daniel Schwarzkopf,[2] V. Ramaswamy,[2] and Michael Oppenheimer[1,3]

Received 22 February 2005; revised 15 September 2005; accepted 6 October 2005; published 24 December 2005.

[1] The global distribution of tropospheric ozone (O_3) depends on the emission of precursors, chemistry, and transport. For small perturbations to emissions, the global radiative forcing resulting from changes in O_3 can be expressed as a sum of forcings from emission changes in different regions. Tropospheric O_3 is considered in present climate policies only through the inclusion of indirect effect of CH_4 on radiative forcing through its impact on O_3 concentrations. The short-lived O_3 precursors (NO_x, CO, and NMHCs) are not directly included in the Kyoto Protocol or any similar climate mitigation agreement. In this study, we quantify the global radiative forcing resulting from a marginal reduction (10%) in anthropogenic emissions of NO_x alone from nine geographic regions and a combined marginal reduction in NO_x, CO, and NMHCs emissions from three regions. We simulate, using the global chemistry transport model MOZART-2, the change in the distribution of global O_3 resulting from these emission reductions. In addition to the short-term reduction in O_3, these emission reductions also increase CH_4 concentrations (by decreasing OH); this increase in CH_4 in turn counteracts part of the initial reduction in O_3 concentrations. We calculate the global radiative forcing resulting from the regional emission reductions, accounting for changes in both O_3 and CH_4. Our results show that changes in O_3 production and resulting distribution depend strongly on the geographical location of the reduction in precursor emissions. We find that the global O_3 distribution and radiative forcing are most sensitive to changes in precursor emissions from tropical regions and least sensitive to changes from midlatitude and high-latitude regions. Changes in CH_4 and O_3 concentrations resulting from NO_x emission reductions alone produce offsetting changes in radiative forcing, leaving a small positive residual forcing (warming) for all regions. In contrast, for combined reductions of anthropogenic emissions of NO_x, CO, and NMHCs, changes in O_3 and CH_4 concentrations result in a net negative radiative forcing (cooling). Thus we conclude that simultaneous reductions of CO, NMHCs, and NO_x lead to a net reduction in radiative forcing due to resulting changes in tropospheric O_3 and CH_4 while reductions in NO_x emissions alone do not.

Citation: Naik, V., D. Mauzerall, L. Horowitz, M. D. Schwarzkopf, V. Ramaswamy, and M. Oppenheimer (2005), Net radiative forcing due to changes in regional emissions of tropospheric ozone precursors, *J. Geophys. Res.*, *110*, D24306, doi:10.1029/2005JD005908.

1. Introduction

[2] The long-term objective of the United Nations Framework Convention on Climate Change (UNFCCC), stated in Article 2 of the accord, is to stabilize greenhouse gas concentrations in the atmosphere at a level that would prevent dangerous anthropogenic interference with the climate system. To achieve this goal, a multitude of policies and measures that cover relevant sources, sinks and reservoirs of greenhouse gases need to be considered. The Kyoto Protocol to the UNFCCC, adopted in 1997, sets binding targets for the sum of emissions of carbon dioxide (CO_2), methane (CH_4), nitrous oxide (N_2O), hydrofluorocarbons (HFCs), perfluorocarbons (PFCs), and sulfur hexafluoride (SF_6) weighted by the Global Warming Potentials (GWPs) of each gas using a 100 year time horizon. Because of their long lifetimes, these greenhouse gases are well mixed in the atmosphere, and their direct effects on the Earth's radiative balance are well quantified and understood with a high level of precision [*Ramaswamy et al.*, 2001]. Other human-influenced chemical species in the atmosphere are not well mixed but nevertheless contribute a significant radiative forcing either directly or through their effects on other

[1]Woodrow Wilson School of Public and International Affairs, Princeton University, Princeton, New Jersey, USA.
[2]Geophysical Fluid Dynamics Laboratory, NOAA, Princeton, New Jersey, USA.
[3]Department of Geosciences, Princeton University, Princeton, New Jersey, USA.

0148-0227/05/2005JD005908$09.00

radiatively active species. Currently, no climate targets have been set for emissions of these species primarily because of the complexity in estimating their global distributions and their climate forcing. Tropospheric ozone (O_3), a direct greenhouse gas and an air pollutant, is a key example. O_3 is not directly emitted and its production depends nonlinearly on the emissions of its precursors (CH_4, nitrogen oxides (NO_x), carbon monoxide (CO), and nonmethane hydrocarbons (NMHCs)), making it difficult to determine the exact amount a country is responsible for producing. O_3 and its short-lived precursors (NO_x, CO, and NMHCs) modify the lifetime of CH_4 by controlling the oxidative capacity of the atmosphere through reactions that produce and consume hydroxyl radical (OH). NO_x, CO and some NMHCs are regulated through national air quality programs and regionally under the Convention on Long-range Transboundary Air Pollution (LRTAP). The radiative effect of O_3 is partly included in the GWP for CH_4, however, O_3 and its short-lived precursors are not directly regulated in a climate mitigation agreement.

[3] Measurements and modeling studies have shown that O_3 concentrations have increased significantly since preindustrial times resulting in a radiative forcing similar to that due to the increase in CH_4 concentration albeit with a greater uncertainty [*Ramaswamy et al.*, 2001]. Approximately 20% of the present CH_4 radiative forcing since preindustrial times is attributed to enhanced levels of O_3 associated with photochemical production from CH_4. The uncertainty in total O_3 forcing is mostly due to uncertainties in the preindustrial O_3 level and its present distribution rather than to factors related to radiative transfer as the radiative properties of O_3 are understood as well as those of CO_2, CH_4, N_2O, and the CFCs [*Berntsen et al.*, 2000; *Gauss et al.*, 2003].

[4] The radiative forcing due to a long-lived greenhouse gas does not vary significantly (on a per molecule basis) with the location of its emissions. Therefore emission inventories that identify the quantity of each long-lived gas emitted by a particular country are sufficient to assign responsibility to that country for the forcing caused by its emissions. This is, however, not the case for tropospheric O_3, a secondary pollutant that is formed photochemically in the atmosphere. The lifetime of O_3, ranging from days to many weeks, is shorter than the mixing time of several months in the troposphere, resulting in a nonuniform distribution in space and time. The short lifetimes of O_3 precursors and the nonlinear dependence of O_3 production on precursor concentrations, particularly NO_x, add to the spatial and temporal variability in O_3 and make it difficult to quantify each country's contribution to the tropospheric O_3 burden. Furthermore, the radiative forcing due to O_3 depends on its vertical distribution, with changes in O_3 concentration near the tropopause resulting in the greatest radiative forcing efficiency on a per molecule basis [*Wang et al.*, 1980; *Lacis et al.*, 1990; *Wang et al.*, 1993; *Forster and Shine*, 1997]. Regional differences in chemical and meteorological conditions have also been shown to cause strong variations in radiative forcing from O_3 [*Berntsen et al.*, 1996; *Haywood et al.*, 1998; *Fuglestvedt et al.*, 1999; *Mickley et al.*, 1999; *Wild et al.*, 2001; *Berntsen et al.*, 2005a]. Attributing responsibility to specific countries for radiative forcing resulting from emissions of tropospheric O_3 precursors is thus not as straightforward as it is for the direct emission of long-lived greenhouse gases, because the radiative forcing depends both on the location of the precursor emissions as well as on where the O_3 is formed and transported. In addition, previous modeling studies have shown that the climate sensitivity to a given radiative forcing due to a change in O_3 may not be the same as for radiative forcing due to a change in CO_2 [*Hansen et al.*, 1997; *Joshi et al.*, 2003].

[5] Recent discussions have focused on whether non-CO_2 greenhouse agents, including O_3 and aerosols, should be included in a greenhouse control strategy for climate mitigation benefits [*Derwent et al.*, 2001; *Holloway et al.*, 2003; *Swart et al.*, 2004; *Rypdal et al.*, 2005]. *Hansen et al.* [2000] have noted the importance of short-lived non-CO_2 greenhouse species in slowing global warming and suggested focusing on air pollutants, especially aerosols and tropospheric O_3, to gain dual benefits from air pollution and climate change mitigation. Including O_3 in a comprehensive climate treaty would require knowledge of the contribution of each country or region's emissions to the global O_3 concentration as well as the corresponding radiative forcing. Initial efforts have been undertaken to understand and quantify these contributions. For example, *Fuglestvedt et al.* [1999] investigated the response of O_3 concentration and its radiative forcing due to a 20% reduction in anthropogenic NO_x emissions from a few selected geographical regions. The study demonstrated that upper tropospheric O_3 concentrations and the resulting O_3 radiative forcing are more sensitive to NO_x reductions in Southeast Asia than in midlatitude and high-latitude regions including Europe, Scandinavia, and the USA. *Berntsen et al.* [2005a] analyzed the impact of changes in emissions of NO_x and CO individually from two regions – Europe and Southeast Asia – and showed that the global O_3 burden and its radiative forcing are more sensitive to emission changes from Southeast Asia than from Europe. Some studies have examined the indirect effects of regional NO_x emissions on CH_4 through changes in the oxidative capacity of the atmosphere and show that the radiative forcings resulting from changes in O_3 and CH_4 nearly offset each other; the sign of the remaining net forcing, however, depends on the region of precursor emission reduction [*Fuglestvedt et al.*, 1999; *Wild et al.*, 2001; *Berntsen et al.*, 2005a].

[6] Since emissions of O_3 precursors from Asian countries (East Asia, Southeast Asia, the Indian Subcontinent) are rising and may continue to rise for several decades, and emissions from Africa and South America may increase in the future because of economic growth [*Akimoto*, 2003], we must carefully evaluate each continent/region's contribution to tropospheric O_3 distributions and resulting climate forcing before including O_3 or any other short-lived species in a climate mitigation treaty. Improved air quality from reduced tropospheric O_3 and its precursor emissions will also benefit human health and ecosystems in addition to mitigating climate change.

[7] In this study, we investigate the sensitivity of global O_3 and CH_4 burdens and forcings to marginal reductions in regional anthropogenic surface NO_x emissions alone and NO_x, CO, and NMHCs emissions together from major geographic regions. We first examine NO_x emissions alone as NO_x is the primary limiting catalyst for O_3 production

[*Lin et al.*, 1988], and it is possible to reduce NO_x emissions from anthropogenic sources without significantly affecting other precursors [*Heinsohn and Kabel*, 1999]. We also examine marginal reductions in the combined emissions of surface anthropogenic NO_x, CO, and NMHCs, because this provides an estimate of the effect of controls on the suite of O_3 precursors. In a series of a three-dimensional global chemical transport model (CTM) perturbation simulations we quantify the change in tropospheric O_3 burden, first, due to a 10% reduction in surface anthropogenic NO_x emissions from Africa, Australia, East Asia, Europe, the Former Soviet Union, the India subcontinent, North America, South America, and Southeast Asia, and second, due to a combined 10% reduction in surface anthropogenic emissions of NO_x, CO, and NMHCs from Europe, North America and Southeast Asia. We select these three regions to represent the distinct meteorological and chemical conditions associated with extratropical and tropical latitudes and the magnitude of emissions ranging from highest (North America) to lowest (Southeast Asia). We estimate the radiative forcing due to the change in tropospheric O_3 concentration resulting from each of the CTM perturbation simulations using a radiative transfer model (RTM). We do not consider perturbations in anthropogenic emissions of CH_4, although CH_4 is an O_3 precursor. Instead we quantify the increase in CH_4 abundance and its radiative forcing as a result of decreases in NO_x, CO, and NMHCs emissions.

[8] Our objective is to quantify the net effect on global radiative forcing of a marginal reduction in anthropogenic emissions of O_3 precursors from each region of the world. These radiative forcings would be useful to compare the climate impact of O_3 precursors with that of CO_2 and would provide policymakers with a basis for crediting countries for reducing their emissions of O_3 precursors, therefore lessening their impact on climate while simultaneously improving local and regional air quality. Section 2 of this paper describes the global three-dimensional CTM, MOZART-2, and the global radiative transfer model. In section 3, we describe the model simulations performed for the analysis. Section 4 presents results from MOZART-2 and RTM calculations. Uncertainties and policy implications of our results are discussed in section 5. Finally, we present conclusions in section 6.

2. Model Description

2.1. MOZART-2

[9] We use the global three-dimensional chemical transport model, Model for Ozone and Related Tracers version 2 (MOZART-2) [*Horowitz et al.*, 2003], to simulate the changes in tropospheric O_3 concentration resulting from a 10% reduction in continental anthropogenic emissions, either of NO_x alone, or of combined NO_x, CO and NMHCs. MOZART-2 simulates the distribution of 63 chemical species from the surface to the lower stratosphere (4 mb) with a horizontal resolution of 2.8° latitude $\times$ 2.8° longitude with 34 hybrid vertical levels, using a time step of 20 minutes for all chemical and transport processes. In this study, we drive MOZART-2 with meteorological variables from the middle atmosphere version of the Community Climate Model (MACCM3) archived every 3 hours. A full description and evaluation of the version of MOZART-2 used here are given by *Horowitz et al.* [2003].

[10] Built on the framework of the transport model MATCH (Model of Atmospheric Transport and Chemistry [*Rasch et al.*, 1997], MOZART-2 accounts for advection, convection, boundary layer transport, surface emissions, photochemistry, and wet and dry deposition. The flux-form semi-Lagrangian advection scheme of *Lin and Rood* [1996] is used for tracer transport. Convective mass fluxes are rediagnosed using the *Hack* [1994] scheme for shallow and midlevel convection and the *Zhang and McFarlane* [1995] scheme for deep convection. Studies have demonstrated that changes in ozone concentration near the tropopause result in the greatest greenhouse forcing efficiency on a per molecule basis [*Wang et al.*, 1980; *Lacis et al.*, 1990; *Wang et al.*, 1993; *Forster and Shine*, 1997]. The vertical distribution of ozone and its precursors, particularly short-lived NO_x species, is determined to a large extent by convective transport of surface pollutants from the boundary layer to the upper troposphere on short (hourly) timescales. Therefore, to evaluate the sensitivity of global radiative forcing to regional air pollution, it is important to accurately represent convective transport. The combination of the *Hack* [1994] and *Zhang and McFarlane* [1995] schemes have been shown to provide a realistic transport of trace species from the surface to the upper troposphere [*Rasch et al.*, 2003].

[11] In MOZART-2 the stratospheric concentration of O_3 is constrained above the local thermal tropopause (defined by a lapse rate of 2 K km^{-1}) by relaxation toward observed O_3 climatologies [*Randel et al.*, 1998; *Logan*, 1999]. Surface emissions of chemical species are taken from the MOZART-2 emission inventory used by *Horowitz et al.* [2003] which is intended to represent the early 1990s. Surface emissions of NO_x include emissions from fossil fuel burning and other industrial activities, biofuel combustion (including fuelwood burning), biomass burning, and biogenic emissions from vegetation and soils. NO_x emissions from fossil fuel and biofuel combustion are based on the Emission Database for Global Atmospheric Research (EDGAR) v2.0 inventory [*Olivier et al.*, 1996]. The global total NO_x emission is 40.8 Tg N/yr with fossil fuel combustion and industrial activities contributing 23.1 Tg N/yr and biofuel consumption resulting in 1.3 Tg N/yr. MOZART-2 also includes aircraft and lightning emissions of NO_x accounting for 0.67 Tg N/yr and 3.0 Tg N/yr, respectively. MOZART-2 simulates the emissions and chemical losses of CH_4; however, the adjustment timescale for CH_4 is sufficiently long (approximately 12 years) that CH_4 does not reach a new steady state within the 2-year simulations conducted here. CH_4 concentrations are thus sensitive to the initial conditions used, which are from a previous simulation of MOZART and agree reasonably with observations. The longer-term adjustment of CH_4, dominated by the tropospheric "primary mode," is treated in section 4.2.

[12] MOZART-2 driven by MACCM3 climatology has been extensively evaluated by comparing results with observations from ozonesondes, aircraft, and surface-monitoring stations and has been shown to simulate the concentrations of tropospheric O_3 and its precursors reasonably well [*Horowitz et al.*, 2003]. A realistic simulation of the distribution of NO_x is particularly important for this

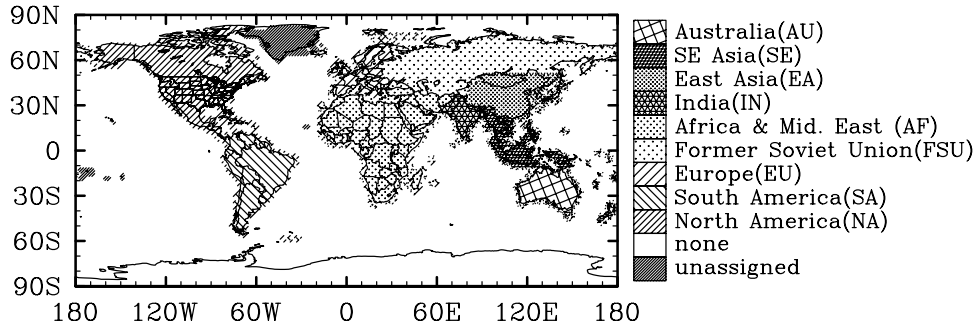

Figure 1. Map of the world showing nine regions where anthropogenic NO_x emissions are reduced by 10% for this study. See color version of this figure at back of this issue.

study because of the nonlinear photochemistry. Comparison of model-simulated vertical profiles of NO_x concentrations with observations from field aircraft campaigns show that MOZART-2 simulates NO_x very well at almost all locations, over a range of concentrations spanning several orders of magnitude [*Horowitz et al.*, 2003].

2.2. GFDL Radiative Transfer Model

[13] Radiative forcing from simulated changes in ozone concentration due to a 10% reduction in regional anthropogenic emissions of O_3 precursors is calculated using the Geophysical Fluid Dynamics Laboratory (GFDL) global three-dimensional radiative transfer model (RTM). The RTM is a component of the new global atmosphere (AM2) and land surface model (LM2) developed at the GFDL for climate research [*GFDL Global Atmospheric Model Development Team*, 2004]. The RTM performs solar and terrestrial radiative transfer calculations. The solar radiative transfer algorithm follows the two-stream δ-Eddington multiple band parameterization of *Freidenreich and Ramaswamy* [1999]. The solar spectrum ranges from 0.2 to 4 μm and is divided into 18 bands to account for the absorption by CO_2, H_2O, O_2, and O_3, molecular scattering, and scattering and absorption by aerosols and clouds. Results from the solar radiation code have been tested against benchmark calculations using the HITRAN catalogue and the maximum error in the clear-sky heating rates is less than 10% [*Freidenreich and Ramaswamy*, 1999]. The terrestrial radiative algorithm is based on the modified version of the Simplified Exchange Approximation (SEA) method developed and evaluated by *Schwarzkopf and Ramaswamy* [1999]. The terrestrial spectrum ranges from 4.55 μm to ∞ to account for the absorption and emission by major atmospheric gases, including H_2O, CO_2, N_2O, O_3, CH_4, and the halocarbons CFC-11, CFC-12, CFC-113 and HCFC-22. Absorption by aerosols and clouds in the longwave is also considered.

[14] In previous studies, the RTM has been used to assess the radiative forcing due to both well-mixed greenhouse gases [*Schwarzkopf and Ramaswamy*, 1999] and short-lived forcing agents (O_3 and aerosols) [*Haywood and Ramaswamy*, 1998; *Haywood et al.*, 1998]. In addition, *Haywood et al.* [1998] show that the radiative forcing due to human-induced changes in tropospheric O_3 calculated using the off-line RTM and the full GCM are in reasonable agreement, suggesting that monthly mean climate variables may be used without introducing significant biases in the calculated radiative forcings.

[15] In the present study, the RTM simulations use archived meteorological fields including insolation, temperature, specific humidity, cloud amount, and surface reflectance that are simulated by AM2/LM2 for the early 1990s. The RTM is run for each grid column of AM2/LM2, which has a horizontal resolution of 2.5° longitude × 2° latitude with 24 vertical levels from the surface to 3 mb. Random cloud overlap is assumed in the model. Concentrations of the well-mixed greenhouse gases are set at values typical of the early 1990s. The tropopause is assumed to vary linearly with latitude from a pressure of 100 mb at the equator to 300 mb at the poles and is zonally invariant (“linear tropopause”).

3. Numerical Simulations

3.1. O_3 Concentration Simulations

[16] We perform a “base case” simulation of MOZART-2 with the standard emission inventory described earlier to obtain a reference chemical state. Similarly, we perform a series of perturbation simulations described below that provide a quantitative estimate of the O_3 changes resulting from potentially feasible reductions in regional emissions of anthropogenic NO_x or combined NO_x, CO, and NMHCs emissions. All simulations are run for 25 months and results for the last 12 months are used for analysis.

[17] We perform MOZART-2 simulations in which surface anthropogenic NO_x emissions from each of the nine regions shown in Figure 1 are reduced by 10%. Similarly, we perform MOZART-2 simulations with combined anthropogenic emissions of NO_x plus CO and NMHCs reduced by 10% for Europe, North America and Southeast Asia. Because of computational constraints, we limit our analysis for combined NO_x, CO, and NMHC reductions to these three regions that represent the distinct meteorological and chemical conditions associated with extratropical and tropical latitudes. Previous modeling studies have suggested that a 10% perturbation in NO_x emissions is small enough to avoid significant nonlinear chemical influence on O_3 production and large enough to produce a measurable response in O_3 [*Wild and Akimoto*, 2001; *Kunhikrishnan and Lawrence*, 2004]. The difference between the global O_3 distributions in a perturbation simulation and the base case indicates the effect of reductions in a region’s precursor emissions. Each region’s anthropogenic NO_x emissions in the base case is presented in column 2 of Table 1a and anthropogenic CO and NMHC emissions are presented in columns 2 and 3 of Table 1b, respectively. The highest

Table 1a. Global Reductions in O_3 Burden and Sensitivity of O_3 Reductions to Regional Reductions in Anthropogenic NO_x Emissions[a]

Region	Anthropogenic NO_x, Tg N yr^{-1}	Total NO_x, Tg N yr^{-1}	ΔO_3, Tg yr^{-1} Short-Lived Mode	ΔO_3, Tg yr^{-1} Primary Mode	ΔO_3, Tg yr^{-1} Total	$\Delta\tau_{CH4}$, years	ΔCH_4, ppb	$\Delta O_3/\Delta E_{NO_x}$, Tg/Tg N yr^{-1}	$\Delta CH_4/\Delta E_{NO_x}$, ppb/Tg N yr^{-1}
Africa and Middle East (AF)	2.0	8.6	−0.24	0.14	−0.10	0.013	3.25	0.51	−16.23
Australia (AU)	0.4	1.1	−0.12	0.06	−0.06	0.006	1.44	1.49	−36.95
East Asia (EA)	4.0	4.8	−0.25	0.12	−0.13	0.011	2.75	0.32	−6.90
Europe (EU)	5.0	5.3	−0.09	0.07	−0.02	0.006	1.55	0.05	−3.22
Former Soviet Union (FSU)	2.5	3.2	−0.07	0.05	−0.02	0.005	1.18	0.07	−4.79
Indian Subcontinent (IN)	1.1	2.1	−0.19	0.08	−0.11	0.007	1.85	0.99	−16.04
North America (NA)	8.0	9.5	−0.46	0.23	−0.23	0.021	5.41	0.29	−6.78
South America (SA)	0.8	4.7	−0.27	0.13	−0.14	0.012	2.99	1.66	−36.00
South East Asia (SE)	0.6	1.4	−0.30	0.13	−0.17	0.012	2.97	2.70	−45.65

[a]Columns 2 and 3 show base surface anthropogenic and total NO_x emissions (Tg N yr^{-1}) for each region, respectively. Columns 4 and 5 show the simulated changes in global total O_3 burden (Tg) associated with short-lived and primary modes (as described in section 4.2), respectively, resulting from a 10% reduction in regional anthropogenic NO_x emissions. Columns 7 and 8 show the estimated changes in CH_4 lifetime and the steady state CH_4 concentration. Changes in O_3 and CH_4 burden normalized with respect to the regional NO_x emission reductions are shown in Columns 9 and 10, respectively.

anthropogenic NO_x emissions are from North America (NA) while the lowest are from Australia (AU). Since emissions from each of these regions are reduced by 10% from the base emissions in the perturbation simulations, the magnitudes of reduction vary across the regions.

3.2. Radiative Flux Calculations

[18] Since MOZART-2 does not simulate O_3 concentration changes in the stratosphere, monthly mean tropospheric O_3 concentrations for the base and perturbed simulations described above are merged with the observed stratospheric O_3 values for 1990 (data compiled from SAGE I + II and ozonesondes by W. Randel (personal communication, 2004)) and then interpolated to the RTM horizontal and vertical grid. The O_3 concentrations are thus only allowed to vary below the linear tropopause and any changes that occur above the linear tropopause are neglected in the RTM. The base and perturbed O_3 distributions are used to perform RTM simulations with meteorological fields from AM2/LM2 sampled for one day per month at midmonth to represent monthly mean conditions. The monthly mean net irradiance (solar and terrestrial) at the tropopause is calculated for the base and perturbed O_3 distributions. ''Instantaneous'' radiative forcings are calculated as the difference in the net irradiance at the tropopause between the perturbed case and the base case. ''Instantaneous'' here implies that we do not allow the stratospheric temperature to adjust to equilibrium after perturbing the surface-troposphere energy budget to account for the changes in the infrared emission from the stratosphere to the troposphere in the radiative forcing [*Intergovernmental Panel on Climate Change* (*IPCC*), 1995; *Fuglestvedt et al.*, 2003]. For some climate mechanisms, such as changes in stratospheric ozone, the distinction between adjusted and instantaneous radiative forcing is crucial as they can be of opposite signs [*Fuglestvedt et al.*, 2003]. For changes in tropospheric O_3, *Haywood et al.* [1998] show that stratospheric adjustment will reduce the instantaneous radiative forcing by only about 10%. Since any changes in O_3 that occur above the linear tropopause are neglected in our MOZART-2 and RTM simulations (see above), stratospheric adjustment is likely to make only a small difference in our results and is unlikely to change the sign of instantaneous radiative forcing calculated here.

4. Results

4.1. Ozone Perturbations Resulting From Regional Emission Reductions

4.1.1. Effect of Anthropogenic NO_x Emission Reduction

[19] Reduced emissions of NO_x, the limiting catalyst in O_3 production in the free troposphere and the marine boundary layer, cause a reduction in O_3 concentration in all but urban areas and high-NO_x plumes. The magnitude and spatial distribution of the O_3 reduction, however, varies with season, the region from which NO_x emissions are reduced and the background levels of NO_x, CO and NMHCs. The vertical distribution of the annual mean O_3 reduction depends on the dynamical regime of the region from which the emissions are reduced (Figure 2). NO_x reductions from tropical regions, including Southeast Asia, the Indian subcontinent, and East Asia result in pronounced O_3 reductions (75–150 pptv) in the middle to upper troposphere that are largely confined to the latitude range

Table 1b. Same as in Table 1a but for a Combined 10% Reduction in Regional Anthropogenic NO_x, CO, and NMHC Emissions[a]

Region	Anthropogenic CO, Tg yr^{-1}	Anthropogenic NMHC, Tg C yr^{-1}	ΔO_3, Tg yr^{-1} Short-Lived Mode	ΔO_3, Tg yr^{-1} Primary Mode	ΔO_3, Tg yr^{-1} Total	$\Delta\tau_{CH4}$, years	ΔCH_4, ppb	$\Delta O_3/\Delta E_{NO_x}$, Tg/Tg N yr^{-1}	$\Delta CH_4/\Delta E_{NO_x}$, ppb/Tg N yr^{-1}
Europe (EU)	69.3	3.5	−0.22	−0.01	−0.23	−0.001	−0.16	0.46	0.34
North America (NA)	100.0	4.7	−0.65	0.12	−0.53	0.011	2.74	0.67	−3.43
Southeast Asia (SE)	41.2	2.6	−0.42	0.09	−0.33	0.010	2.16	5.04	−33.15

[a]Columns 2 and 3 show base regional surface anthropogenic CO and NMHC emissions.

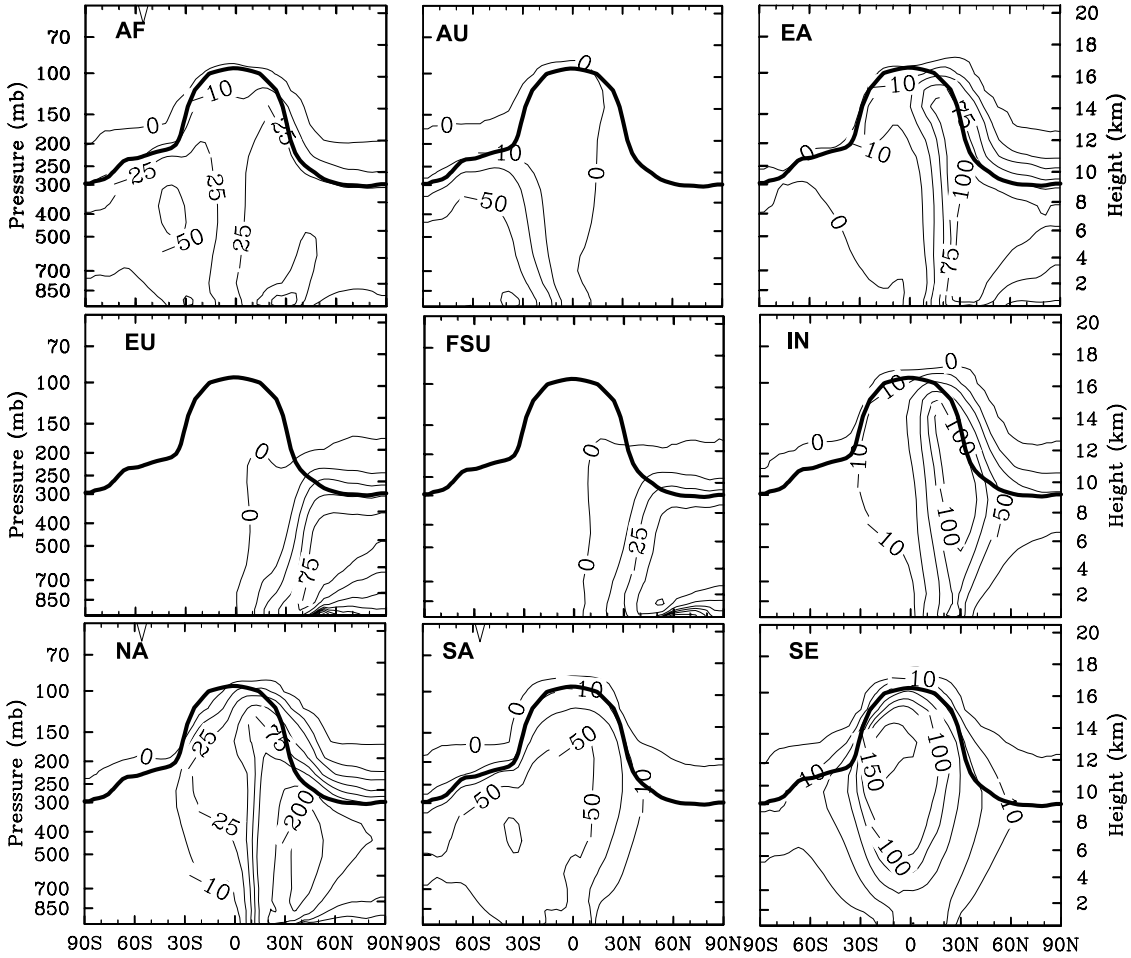

Figure 2. Simulated changes in zonal and annual average O_3 mixing ratio (pptv) due to a 10% reduction in surface anthropogenic NO_x emissions from each of the nine regions shown in Figure 1. Bold lines show the 150 ppb O_3 level from the base case simulation which is used a proxy for the tropopause height (see discussion in section 4.1.1).

of the source region. These tropical regions are characterized by deep convective activity that results in rapid transport of O_3 and its precursors from the boundary layer to the upper troposphere where ozone production efficiency is higher. Reductions in anthropogenic NO_x emissions from Africa and South America also result in O_3 decreases in the middle troposphere; however, the reductions are smaller and spread out because these source regions do not have strong convection so O_3 and its precursors remain at lower altitude. NO_x reductions from midlatitude regions, including Australia, Europe, the Former Soviet Union and North America result in the largest decreases in O_3 in the midtroposphere (2–8 km) with perturbations extending poleward. The largest reductions in O_3 results from 10% reductions in NO_x emissions from North America because the absolute magnitude of emissions from North America is the largest.

[20] Figure 3 shows the change in the annually averaged tropospheric O_3 column due to 10% NO_x emission reductions for each of the nine regions. The tropospheric O_3 column is calculated from the surface up to the model vertical level at which O_3 concentration equals 150 ppbv in the base simulation following *Prather et al.* [2001]. Short lifetimes of O_3 and its precursors and regional differences in transport timescales result in significant spatial gradients in the O_3 perturbations. The largest column reductions occur locally near the source of the emissions; however, the plume of reduced O_3 column extends zonally. For North America and East Asia, the regions of reduced O_3 column extend across the Atlantic and Pacific Ocean, respectively. The horizontal long-range transport of O_3 and its precursors from these regions has been shown to be efficient especially in spring and autumn when the boundary layer O_3 production and vertical lifting are greater than in winter [*Wild and Akimoto*, 2001]. For Europe, Former Soviet Union and Australia, the reduced O_3 regions are less diffuse. The perturbed O_3 column shows a dipole over Europe, with a small increase in O_3 column over northwestern Europe but a reduction over Eastern Europe. Small reductions in industrial NO_x emissions from polluted areas of northwestern Europe result in less wintertime titration of O_3 as shown by *Wild and Akimoto* [2001] and cause O_3 columns to increase (up to 5×10^{-2} DU). Locally, the peak O_3 column decrease from emission reductions in South America, Southeast Asia, and the Indian subcontinent are similar to that from North America (0.4–0.6 DU), although anthropogenic NO_x emitted from these regions is less than half that emitted from

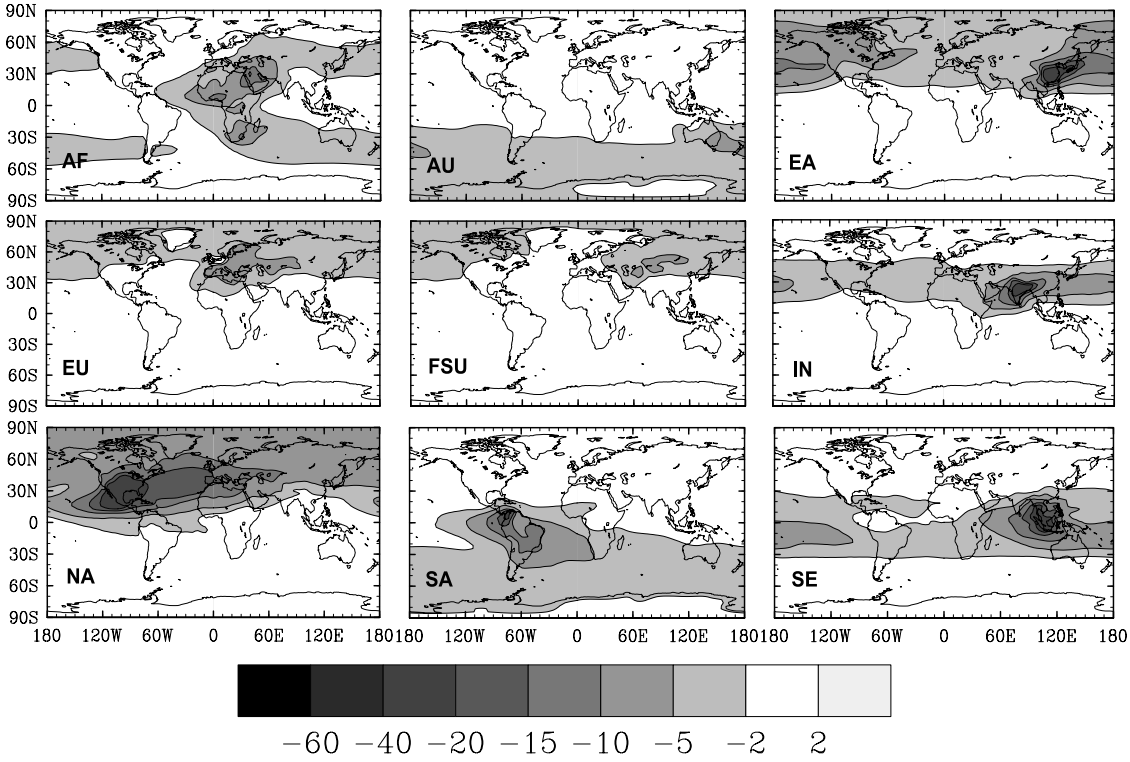

Figure 3. Simulated changes in annual column tropospheric O_3 (10^{-2} DU) due to a 10% reduction in surface anthropogenic NO_x emissions from each of the nine regions. See color version of this figure at back of this issue.

North America (Table 1a). High photochemical and convective activity throughout the year accompanied by relatively high VOC/NO_x concentration ratios resulting in part from biomass burning lead to more efficient O_3 production in tropical than midlatitude regions. The changes in global O_3 burden range from −0.23 Tg for North America to −0.02 Tg each for Europe and Former Soviet Union (Table 1a and Figure 4a). The sensitivity of global O_3 burden to a region's NO_x emissions, calculated as the normalized change in global O_3 burden per unit change in NO_x emissions ($\Delta O_3/\Delta E_{NOx}$), is highest for low NO_x emitting tropical regions (Southeast Asia, South America and Australia) and lowest for high NO_x emitting midlatitude and high-latitude regions with concentrated emissions (Europe, the Former Soviet Union; Figure 4b and Table 1a). The sensitivity of global O_3 change to NO_x reduction from Southeast Asia is almost 9 times higher than that from North America (Figure 4b). The sensitivities calculated for NO_x emission reductions from the Indian subcontinent and East Asia are lower than for other tropical regions because of higher background NO_x emissions from these regions.

[21] There are large differences in the seasonal cycle of the O_3 perturbations. The monthly variations in global O_3 changes are shown for both the surface (Figure 5a) and upper troposphere (approximately 12 km; Figure 5b). Surface O_3 is important for air quality issues while upper troposphere O_3 is important for climate forcing (see section 4.3). The seasonal cycle in O_3 perturbation is driven by the seasonality in photochemistry and convective activity with a maximum during summer (Figure 5a). In the Northern Hemisphere, global surface O_3 is reduced by 0.03 to 0.07 ppb during summer months because of the 10% NO_x reductions from extratropical regions (North America, Europe, Former Soviet Union, and East Asia; Figure 5a). The summer peak is attributed to high photochemical activity and O_3 production efficiency as shown in

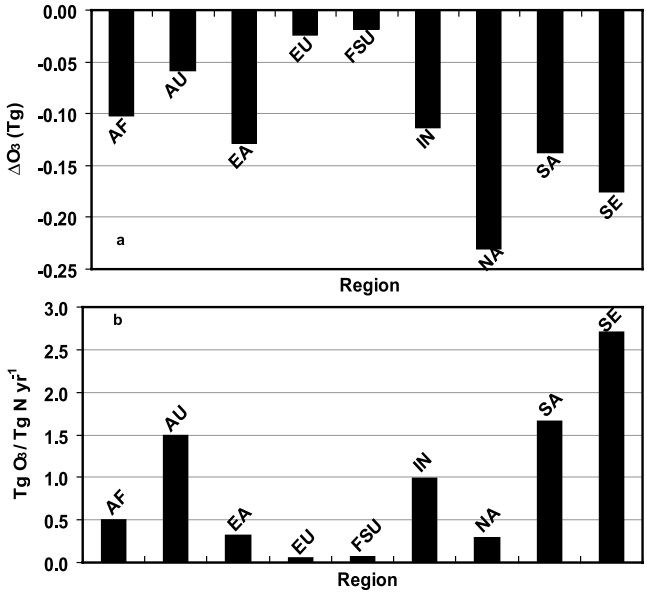

Figure 4. Change in global and annual (a) tropospheric O_3 burden and (b) normalized global O_3 burden ($\Delta O_3/\Delta E_{NO_x}$) due to a 10% reduction in surface anthropogenic NO_x emission from each of the nine regions. These values include contribution to O_3 from the long-lived primary mode (see section 4.2.1).

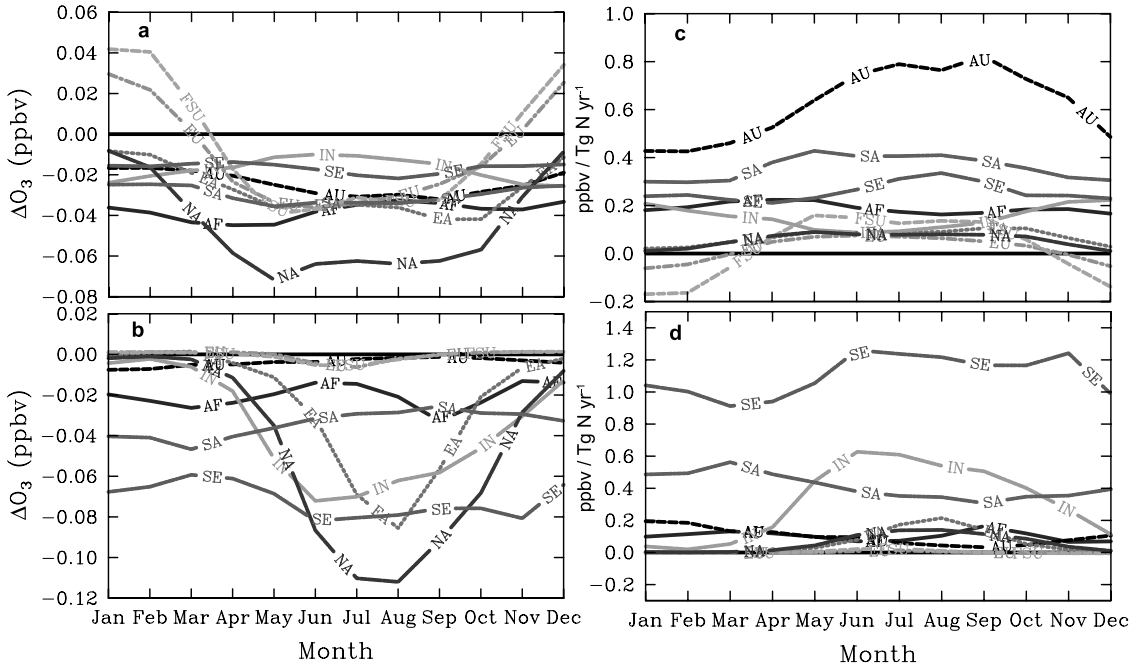

Figure 5. Monthly variation in global O_3 perturbations at (a) surface and (b) 12 km and normalized global O_3 perturbations ($\Delta O_3/\Delta E_{NO_x}$) at (c) surface and (d) 12 km, due to a 10% reduction in surface anthropogenic NO_x emissions from each of the nine regions. See color version of this figure at back of this issue.

Figure 5c [*Hirsch et al.*, 1996]. Within the United States, O_3 production is primarily NO_x limited during summer and becomes HO_x limited in other seasons [*Jacob et al.*, 1995]. During winter the O_3 perturbation is small because of low photochemical activity. Reductions in NO_x emissions from Europe and the Former Soviet Union result in an increase in O_3 due to less wintertime titration of O_3 by NO_x particularly near the source of precursor emissions. There is negligible seasonality in surface O_3 for NO_x reductions from the Indian subcontinent, Southeast Asia, and South America because these equatorial regions experience relatively constant insolation throughout the year. The surface O_3 reductions are smaller than those for midlatitude regions because of lower NO_x emissions, resulting in higher sensitivity to NO_x reductions as shown in Figure 5c. It is difficult to analyze the seasonality of O_3 reduction from Africa because anthropogenic NO_x emissions are quite small and are located in both the northern and the Southern Hemispheres. Furthermore, Africa is strongly influenced by emissions from biomass burning with peak intensities during January–March north of the equator and August–November in the Southern Hemisphere. Lower NO_x emissions combined with emissions of precursors from biomass burning for Africa increase the VOC/NO_x concentration ratio resulting in enhanced O_3 sensitivity at the surface compared with sensitivities to NO_x reductions from North America, Europe and the Former Soviet Union (Figure 5c). The highest sensitivity to NO_x reduction is simulated for Australia where anthropogenic NO_x emissions are the smallest. A cleaner environment and high VOC/NO_x ratio due to biomass burning from May to October make this region strongly NO_x limited.

[22] The seasonality in global O_3 reductions is enhanced in the upper troposphere, particularly for North America, East Asia, and India (Figure 5b). For Europe and the Former Soviet Union, O_3 reductions at 12 km appear to be close to zero throughout the year (in part because 12 km lies in the stratosphere at these latitudes). Convection over Europe and the Former Soviet Union (particularly in the western part where most anthropogenic emissions are located) is weak and O_3 production and destruction occurs mostly in the lower to middle troposphere (Figure 2). For North America and East Asia, vertical transport is important during summer resulting in large O_3 reductions over these regions in the upper troposphere. O_3 reductions are enhanced in the upper troposphere as compared to the surface for NO_x emission reductions from Southeast Asia, South America and the Indian subcontinent and show seasonality associated with convective activity. The Indian subcontinent, particularly, shows significant O_3 reduction during the summer monsoons when deep convection lifts the pollutants to high altitudes where low-NO_x conditions result in high O_3 production efficiencies [*Berntsen et al.*, 1996; *Wild and Akimoto*, 2001]. Small O_3 reductions are simulated for Australia and Africa at upper levels.

[23] We find global O_3 reductions in the upper troposphere to be most sensitive to NO_x emission reductions from tropical regions (Southeast Asia, South America and the Indian subcontinent), with highest sensitivity calculated for Southeast Asia (Figure 5d). We find low sensitivities for NO_x emission reductions from midlatitude and high-latitude regions with lowest sensitivity for Europe and the Former Soviet Union. The sensitivities of upper tropospheric O_3 to NO_x emissions calculated here are consistent with the study of *Fuglestvedt et al.* [1999] who reduced anthropogenic NO_x emissions by 20% and found the sensitivity to be highest for Southeast Asia followed by Australia and lowest for Scandinavia.

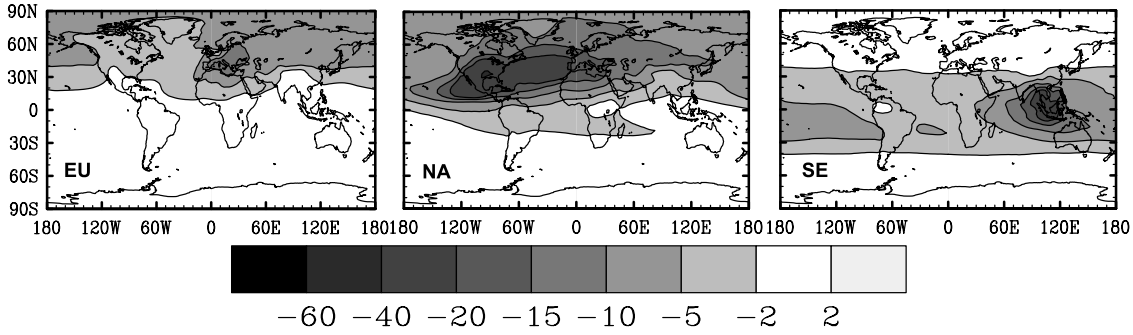

Figure 6. Simulated changes in annual column tropospheric O_3 (10^{-2} DU) due to a combined 10% reduction in surface anthropogenic NO_x, CO, and NMHC emissions from three regions. See color version of this figure at back of this issue.

4.1.2. Effect of Anthropogenic NO_x, CO, and NMHC Emission Reduction

[24] Annually averaged O_3 columns are reduced as a result of combined 10% reductions in anthropogenic emissions of NO_x, CO, and NMHCs for Europe, North America and Southeast Asia (Figure 6 and Table 1b). For the three regional emission perturbations, reducing CO and NMHCs in addition to NO_x slightly reduces the spatial inhomogeneity in the perturbed O_3 column because of the relatively longer lifetime of CO (approximately 2 months) compared with NO_x (compare Figures 6 and 3). The general spatial pattern of regional horizontal gradients, however, is still the same with higher localized column reductions. Compared with NO_x emission reduction only, the maximum reduction in column O_3 from combined reductions in NO_x, CO, and NMHC emissions is enhanced by 0.06, 0.05, 0.03 DU for North America, Europe and Southeast Asia, respectively. For Europe, combined reductions in emissions of NO_x, CO, and NMHCs result in an overall reduction in O_3 column in contrast to the small increase simulated over northwestern Europe for NO_x emission reductions alone. The total reduction in O_3 burden for the combined emission reductions is largest for North America (Table 1b). We expect that combined reductions in emissions of NO_x, CO, and NMHCs from each of the remaining six regions of the world would reduce the global O_3 burden; however, the distribution of O_3 reductions would depend on the location and chemical regime of the source region.

4.2. Methane Increases Resulting From Regional Emission Reductions

4.2.1. Effect of Anthropogenic NO_x Emission Reductions

[25] A reduction in NO_x emissions decreases the oxidizing capacity of the atmosphere by decreasing hydroxyl radical (OH) concentrations and therefore increases the lifetime of CH_4 in the atmosphere [*Prather*, 1994]. The lower OH results from a decreased source of odd-hydrogen ($HO_x = OH + HO_2 + RO_2$) radicals (from photolysis of O_3 followed by reaction of $O(^1D)$ with water vapor), and from decreased recycling of peroxy radicals back to OH. In addition, there is a positive feedback between CH_4 and OH by which the increase in CH_4 causes OH to decrease further, increasing CH_4. Reductions in O_3 and OH resulting from NO_x reductions are readily captured in 2 year MOZART simulations because of the short adjustment times for these species ("short-lived mode"). Perturbations in CH_4 induced by changes in OH, however, approach steady state with an e-folding time of approximately 12 years [*Prather*, 1994, 1996; *Derwent et al.*, 2001; *Prather et al.*, 2001; *Wild et al.*, 2001]. As CH_4 increases toward its new steady state (not captured in our 2-year CTM simulations), the peroxy radical production rises, enhancing O_3 production in response to this "primary mode" of the tropospheric photochemistry system [*Prather*, 1996; *Wild and Prather*, 2000; *Derwent et al.*, 2001; *Wild et al.*, 2001].

[26] Calculating the perturbed steady state CH_4 concentration would require significantly longer and more expensive simulations of MOZART than performed here. *Fuglestvedt et al.* [1999], however, suggested a method to calculate the steady state CH_4 perturbations on the basis of the initial changes in CH_4 lifetime calculated from the shorter simulations. Using this method, we estimate the steady state CH_4 concentration change $\Delta[CH_4]$ as:

$$\Delta[CH_4] = F_{CH_4} * [CH_4]_0 \frac{\Delta\tau}{\tau_0},$$

where τ_0 is the lifetime of CH_4 versus reaction with tropospheric OH in the base simulation which is 9.0 yr in our model, $\Delta\tau$ is the change in CH_4 lifetime for the perturbation simulations, $[CH_4]_0$ is the CH_4 concentration in the base simulation and F_{CH4} is a feedback factor that quantifies the positive feedback between CH_4 and OH described above and is expressed as the ratio of adjustment time to lifetime of CH_4 [*Schimel et al.*, 1996; *Ramaswamy et al.*, 2001]. F_{CH4} is model-dependent and its calculation requires expensive multidecadal simulations of MOZART-2 which are not currently feasible. We therefore use the value of 1.4 recommended by *Prather et al.* [2001]. This long-term increase in CH_4 leads to an increase in O_3, which partially offsets the NO_x-induced decrease in O_3 described above. To quantify this increase in O_3, we use results from the OXCOMP experiment [*Prather et al.*, 2001; *Gauss et al.*, 2003], following *Berntsen et al.* [2005a]. In OXCOMP, the change in global mean tropospheric O_3 in response to a 10% increase in CH_4 was calculated by six global 3-D CTMs to be 0.64 DU (overestimated by about 25 to 33% as

it includes some contribution from O_3 changes in the lower stratosphere [*Prather et al.*, 2001]). We use this average O_3 response to estimate $(\Delta O_3)_{\text{primary}}$, on the basis of the steady state CH_4 change $\Delta[CH_4]$ as:

$$(\Delta O_3)_{primary} = \frac{\Delta[CH_4]}{[CH_4]} \times \frac{0.64}{0.1} DU$$

[27] Columns 4 and 5 of Table 1a show the perturbation in O_3 burden from the short-lived mode (immediate reduction in O_3 from NO_x emissions reduction) and long-lived primary mode (increase in O_3 caused by an increase in CH_4 at steady state), and the total change in O_3 burden as a sum of the short-lived and primary modes is shown in column 6. As shown in columns 7 and 8 of Table 1a, there are regional differences in the response of CH_4 lifetime and its steady state concentration to a 10% reduction in NO_x emissions. We have estimated the global, annual mean change in steady state CH_4 resulting from perturbed emissions; however, this perturbation in CH_4 has a spatially and temporally varying distribution as noted by previous studies [*Wild and Prather*, 2000; *Derwent et al.*, 2001]. The largest increase in the steady state concentration of CH_4 is for NO_x reductions from North America and the smallest for the Former Soviet Union. The normalized CH_4 changes per unit NO_x emissions (column 10 of Table 1a) indicate that as for O_3, CH_4 change is most sensitive to changes in NO_x emissions from low-NO_x regions (Southeast Asia, South America and Australia) and least sensitive to high-NO_x regions (Europe and the Former Soviet Union). The least sensitive regions are also characterized by low photochemical activity.

4.2.2. Effect of Anthropogenic NO_x, CO, and NMHC Emission Reductions

[28] The long-lived primary mode changes in O_3 and CH_4 are diminished when regional CO and NMHCs emissions are reduced in addition to NO_x emissions (columns 5 and 8 of Table 1b). Reaction with OH is the primary loss mechanism for CO and NMHCs in the atmosphere; hence reduced CO and NMHC emissions tend to increase OH, opposing the NO_x-induced decrease in OH. For emission reductions from Europe, CO and NMHC reductions offset the effect of NO_x reductions, resulting in a change in sign (decreases) of the steady state CH_4 concentration change and the primary mode O_3 change (decrease) compared with NO_x reduction alone. For emission reductions from North America and Southeast Asia, a net increase in CH_4 remains resulting in an increase in the primary mode O_3, although, only by about half as much as the increase from NO_x emission reductions alone.

4.3. Radiative Forcing Due to Perturbed Ozone and Methane

4.3.1. Effect of Regional Anthropogenic NO_x Emission Reductions

[29] The annual instantaneous total-sky radiative forcing due to short-lived O_3 changes for the simulations with reduced NO_x emissions is shown in Figure 7. The spatial pattern of the forcings mostly reflects the distribution of annual O_3 column change simulated for each region (Figure 3), but the horizontal gradients in the forcings are stronger than in the O_3 column changes. The region of maximum forcing reduction for each simulation is located near the source of NO_x emissions and the region of maximum O_3 reduction. There is a systematic shift in the maximum radiative forcing reductions toward lower latitudes because of the larger contrast between surface and upper tropospheric temperatures, in the tropics versus at the poles [*Haywood et al.*, 1998]. The reduced forcing extends to other regions following the plume of O_3 reductions. For example, the forcing from North America extends across the Atlantic into Europe and northern Africa. Emission reductions from most regions induce forcing reductions in both hemispheres except for reductions from the Former Soviet Union, Europe, and Australia for which reduced forcing occurs only in their respective hemispheres. Locally, maximum negative radiative forcing from Southeast Asia, South America and the Indian subcontinent is similar to that from North America. Significant O_3 reductions occur near the tropopause for emission reductions from these tropical regions (Figure 2) where O_3 is most radiatively effective leading to large forcings from these regions. The dipole pattern simulated for the O_3 column for emission reductions from Europe is not replicated for the radiative forcing reduction, possibly because the O_3 column change is determined by increases in the boundary layer while radiative forcing is influenced by changes occurring near the tropopause.

[30] Figure 8 shows the monthly variation in the global average O_3 radiative forcing from regional NO_x emission reductions. The seasonal cycle in the simulated radiative forcings is due to the monthly variation in the vertical distribution of O_3 perturbations and can be explained by the seasonality in the global O_3 reduction in the upper troposphere (Figure 5b). Seasonally uniform O_3 changes in the upper troposphere resulting from NO_x emission reductions from tropical regions (Southeast Asia, South America, and Africa) result in nearly constant yearly forcings while emission reductions from high-latitude and midlatitude regions (North America, Europe, the Former Soviet Union) result in peak negative radiative forcings during summer months consistent with maximum upper tropospheric O_3 perturbations simulated during summer. Emission reductions from the Indian subcontinent and East Asia also result in peak radiative forcing reductions during summer associated with O_3 reductions in the upper troposphere resulting from strong convective activity.

[31] The global annual radiative forcings due to O_3 and CH_4 changes are summarized in Figure 9a and Table 2, and the normalized forcing per unit NO_x ($\Delta F_{O3}/\Delta E_{NO_x}$) is shown in Figure 9b. The radiative forcing for O_3 in Table 2 includes contribution from the short-lived (described above) and long-lived primary modes. We calculate the primary mode O_3 forcing for each perturbation by first calculating the global average O_3 forcing per Dobson unit, on the basis of the short-lived mode changes averaged over all emission reduction regions (0.045 Wm^{-2}/DU). This forcing efficiency is then scaled by the primary mode O_3 column change estimated for each emission reduction region. Our calculated average short-lived mode O_3 forcing per Dobson unit change lies within the range of 0.033 to 0.056 Wm^{-2}/DU given by *Ramaswamy et al.* [2001]. The strongest global O_3 radiative forcing from NO_x emission reductions is for Southeast Asia (-1.24 mWm^{-2}), with the weakest for Europe and the Former Soviet Union (-0.03 mWm^{-2}). The O_3 radiative

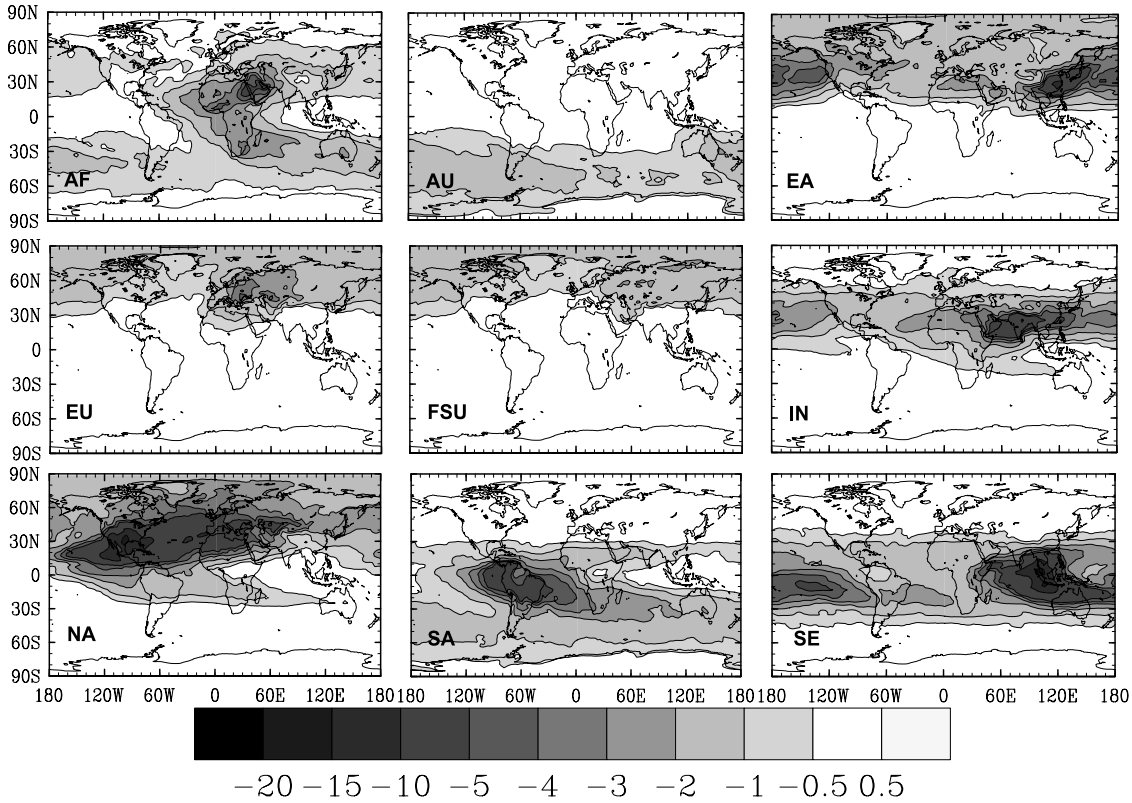

Figure 7. Annual total-sky instantaneous radiative forcing at the tropopause due to short-lived O_3 perturbations resulting from a 10% reduction in surface anthropogenic NO_x emissions from each of the nine regions. See color version of this figure at back of this issue.

forcing per unit NO_x is 15 times higher for Southeast Asia than for North America (Figure 9b). *Fuglestvedt et al.* [1999] calculated the sensitivity of O_3 forcing to NO_x emission reductions to be highest for Southeast Asia and lowest for Scandinavia and the USA, without accounting for the primary mode effect on O_3 concentrations. Their calculated O_3 radiative forcing per unit NO_x reduction was about 7 times higher for Southeast Asia than for the USA, while our calculated O_3 forcing sensitivity is 11 times higher for Southeast Asia than for North America O_3 (short-lived mode only). Differences in the definition of regions and the simulated vertical O_3 distribution can possibly explain the differences in our results compared with the results of *Fuglestvedt et al.* [1999].

[32] NO_x reductions enhance the lifetime and burden of atmospheric CH_4 as described in section 4.2.1. We calculate the radiative forcing due to CH_4 increases resulting from 10% NO_x emission reductions for the nine simulations on the basis of the CH_4 changes in Tables 1a and 1b using the simple formulation described by *IPCC* [1990]. We use this formulation because we cannot conduct MOZART-2 simulations that fully account for the CH_4 concentration increases in response to emission reductions. The results are shown in Table 2 and Figure 9a. The CH_4 forcing is largest for NO_x emission reductions from North America and smallest for the Former Soviet Union. The net radiative forcing from O_3 and CH_4 changes is positive for NO_x emission reductions from all regions (column 4 of Table 2). This indicates that reducing NO_x emissions alone, from any region in the world, results in a small net warming. Our results are consistent with previous studies that have either shown or suggested a similar offsetting effect of CH_4 to NO_x-induced changes in O_3 [*Fuglestvedt et al.*, 1999; *Kheshgi et al.*, 1999; *Mayer et al.*, 2000; *Derwent et al.*, 2001; *Wild et al.*, 2001; *Wigley et al.*, 2002; *Berntsen et al.*, 2005a].

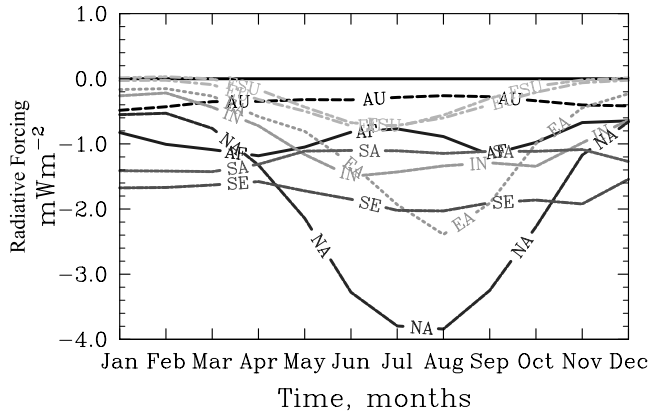

Figure 8. Monthly variation in global instantaneous radiative forcing due to short-lived O_3 perturbations resulting from 10% reduction in surface anthropogenic NO_x emissions from each of the nine regions. See color version of this figure at back of this issue.

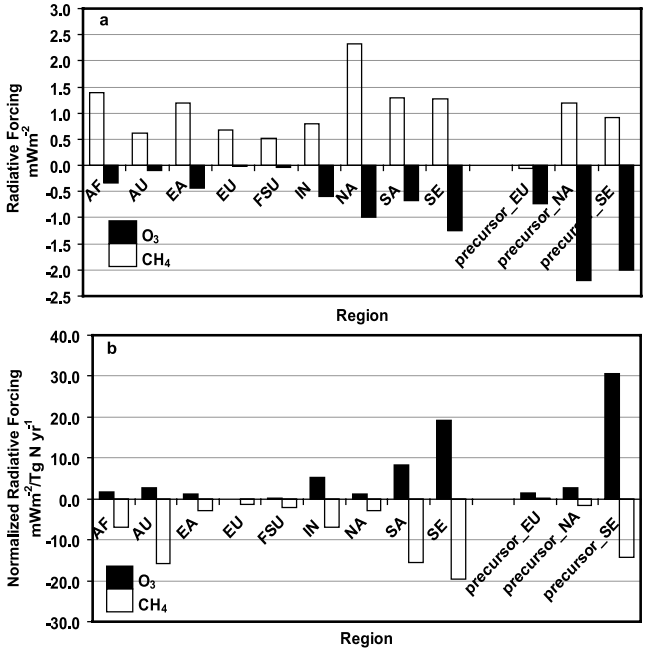

Figure 9. Change in annual (a) absolute radiative forcing and (b) normalized radiative forcing ($\Delta F/\Delta E_{NO_x}$), due to changes in O_3 (short-lived mode plus primary mode) and CH_4 resulting from a 10% reduction in surface anthropogenic NO_x emissions from each of the nine regions and a combined 10% reduction in anthropogenic NO_x, CO, and NMHCs emissions (three bars on the right).

4.3.2. Effect of Regional Anthropogenic NO_x, CO, and NMHC Emission Reductions

[33] Total O_3 forcing (short-lived plus primary mode) becomes more negative when CO and NMHC emissions are decreased in addition to NO_x, while the increase (or in one case decrease) in forcing due to CH_4 changes is less (see the three bars in the right corner of Figure 9a and Table 2). The largest negative global O_3 radiative forcing is simulated for North America and the smallest for Europe. The sensitivity of O_3 to NO_x emissions is further enhanced for Southeast Asia when CO and NMHC emissions are also reduced (Figure 9b). The combined emissions reductions from the regions considered here lead to a net negative global radiative forcing, indicating a net cooling. These results are conceptually consistent with the modeling study of *Wild et al.* [2001] who demonstrated that combined increases in NO_x and CO yields a net positive radiative forcing due to O_3 and CH_4 changes, while increases in NO_x alone result in a net negative forcing with the magnitude depending on the region.

5. Discussion

[34] Overall, MOZART-2 simulates the global distributions of O_3 and its precursors reasonably well. However, MOZART-2 has been shown to overestimate O_3 in the upper troposphere at middle to high northern latitudes, possibly because of excess stratosphere to troposphere exchange [*Horowitz et al.*, 2003]. This and other biases in the base simulation may introduce uncertainties in our results. We have not considered changes in biomass burning emissions, even though these are mostly controlled by humans particularly in the tropics. The effects of biomass burning emissions will be addressed in a future study (V. Naik et al., manuscript in preparation, 2005). We have also not applied emission perturbations to aircraft sources that may have larger impacts on upper tropospheric O_3 from direct emissions in the region.

[35] A direct comparison of the global O_3 and CH_4 forcings does not give a realistic picture of potential climate effects of O_3 precursors because both O_3 and CH_4 respond to changes in emissions on very different temporal and spatial scales [*Wild et al.*, 2001]. O_3 and its forcing respond on a very short timescale (several weeks) via the short-lived mode. CH_4 responds via the primary tropospheric mode on a longer timescale ($\sim$12 years) causing further O_3 changes on this longer timescale. The radiative forcing from the short-lived O_3 mode is regional, while forcing from CH_4 and O_3 due to the long-lived primary mode is relatively homogenous. The climate response to regional forcings will likely differ from the response to a well-mixed greenhouse gas that has a more globally uniform forcing. These basic differences in the temporal and spatial behavior of O_3 and CH_4 forcings complicate our estimate of the net climate forcing from perturbed regional emissions of O_3 precursors.

[36] The magnitude of the net radiative forcing from changes in O_3 and CH_4 simulated for a 10% reduction in regional O_3 precursor emissions is small (the net forcing for the emission reductions we examined for each region is three orders of magnitude smaller than the global present-day radiative forcing due to O_3 of 0.35 Wm^{-2} [*Ramaswamy et al.*, 2001]). However, we are only examining the marginal

Table 2. Global Instantaneous Cloudy-Sky Radiative Forcings Due to Changes in Global O_3 (Short-Lived Mode Plus Primary Mode) and CH_4 Concentrations Resulting From a 10% Regional Reduction of Anthropogenic NO_x Emissions for the Nine Geographical Regions Considered in the Study

Region	ΔF O_3, mWm^{-2}	ΔF CH_4, mWm^{-2}	Net ΔF, mWm^{-2}
Africa & Middle East (AF)	−0.33	1.40	1.07
Australia (AU)	−0.10	0.62	0.52
East Asia (EA)	−0.43	1.19	0.76
Europe (EU)	−0.03 (−0.74)[a]	0.67 (−0.06)[a]	0.64 (−0.80)[a]
Former Soviet Union (FSU)	−0.03	0.51	0.48
Indian Subcontinent (IN)	−0.59	0.80	0.21
North America (NA)	−0.99 (−2.20)[a]	2.33 (1.19)[a]	1.34 (−1.01)[a]
South America (SA)	−0.68	1.29	0.61
South East Asia (SE)	−1.24 (−2.00)[a]	1.28 (0.92)[a]	0.04 (−1.08)[a]

[a]Results from combined reductions in NO_x, CO, and NMHCs.

effect of a small reduction (10%) in the anthropogenic emissions from individual continents – each reduction considered is less than 2% of the total global anthropogenic emissions of O_3 precursors. This unsurprisingly results in small perturbations in O_3 and CH_4 burdens and forcings. For comparison, reductions in aggregate anthropogenic CO_2 equivalent emissions of the long-lived greenhouse gases agreed under the Kyoto Protocol are only 5% below 1990 levels for developed countries resulting in a relatively small decrease in radiative forcing. For a 10% reduction in European emissions of CO_2 and air pollutants, *Berntsen et al.* [2005b] calculated the net climate forcing due to O_3 reductions to be approximately an order of magnitude smaller than that due to CO_2 reductions.

6. Conclusions

[37] In this study, we quantified the global change in tropospheric O_3 and CH_4 burdens and the associated radiative forcing resulting from regional emissions of O_3 precursors (NO_x, CO, and NMHCs). We evaluated the response of O_3 and CH_4 to reduced anthropogenic NO_x emissions alone for nine geographical regions individually and to a combined reduction in anthropogenic emissions of NO_x, CO and NMHCs from three regions, using chemical transport model simulations. We show that O_3 and CH_4 forcings are most sensitive to emission changes from tropical regions (Southeast Asia) and least sensitive to emission changes from midlatitude and high-latitude regions (Europe and North America). The range of normalized forcings found in our analysis suggests that control strategies that reduce emissions of O_3 precursors from tropical regions in particular can have a significant impact on the net climate forcing from O_3 and CH_4. We find that from all regions of the world, reductions in NO_x emissions alone result in a positive forcing from increased CH_4 that dominates over the small negative forcing from decreased O_3 for each region, implying a net warming. Combined reductions in anthropogenic NO_x, CO, and NMHC emissions result in a stronger negative forcing from decreased O_3 and a weaker positive forcing from CH_4, producing a net negative forcing (cooling).

[38] The analysis presented here may prove useful in incorporating tropospheric O_3 and its precursors in a future climate treaty to gain climate change benefits. Since we find that NO_x emission reductions alone are insufficient to produce a net negative radiative forcing, it may therefore be useful to assess the cost effectiveness and political feasibility of including the basket of O_3 precursors in a future climate agreement. Consideration of a climate treaty seeking to obtain cobenefits from reducing radiative forcing and mitigating air pollution could benefit from further studies pertinent to crediting simultaneous reductions of regional emissions of NO_x, CO, and NMHCs, or possibly from CO and NMHCs alone.

[39] **Acknowledgments.** V. Naik was supported by the Carbon Mitigation Initiative (CMI) of the Princeton Environmental Institute at Princeton University (http://www.princeton.edu/~cmi) which is sponsored by BP and Ford. We thank Michael Prather for helpful discussions and Jan Fuglestvedt, Terje Berntsen and an anonymous reviewer for valuable comments on an earlier version of the manuscript. The Geophysical Fluid Dynamics Laboratory provided necessary computational resources.

References

Akimoto, H. (2003), Global air quality and pollution, *Science*, *302*, 1716–1719.

Berntsen, T. K., I. S. A. Isaksen, W.-C. Wang, and X.-Z. Liang (1996), Impacts of increased anthropogenic emissions in Asia on tropospheric ozone and climate, *Tellus, Ser. B*, *48*, 13–32.

Berntsen, T. K., G. Myhre, F. Stordal, and I. S. A. Isaksen (2000), Time evolution of tropospheric ozone and its radiative forcing, *J. Geophys. Res.*, *105*, 8915–8930.

Berntsen, T. K., J. S. Fuglestvedt, M. M. Joshi, K. P. Shine, N. Stuber, M. Ponater, R. Sausen, D. A. Hauglustaine, and L. Li (2005a), Climate response to regional emissions of ozone precursors: Sensitivities and warming potentials, *Tellus, Ser. B*, *57*, 283–304.

Berntsen, T. K., J. S. Fuglestvedt, G. Myhre, F. Stordal, and T. F. Berglen (2005b), Abatement of greenhouse gases: Does location matter?, *Clim. Change*, in press.

Derwent, R. G., W. J. Collins, C. E. Johnson, and D. S. Stevenson (2001), Transient behavior of tropospheric O_3 precursors in a global 3-D CTM and their indirect greenhouse effects, *Clim. Change*, *49*, 463–487.

Forster, P. M. de F., and K. P. Shine (1997), Radiative forcing and temperature trends from stratospheric ozone changes, *J. Geophys. Res.*, *102*, 10,481–10,857.

Freidenreich, S. M., and V. Ramaswamy (1999), A new multiple-band solar radiative parameterization for general circulation models, *J. Geophys. Res.*, *104*, 31,389–31,409.

Fuglestvedt, J. S., T. K. Berntsen, I. S. A. Isaksen, H. Mao, X.-Z. Liang, and W.-C. Wang (1999), Climatic forcing of nitrogen oxides through the changes in tropospheric ozone and methane; global 3D model studies, *Atmos. Environ.*, *33*, 961–977.

Fuglestvedt, J. S., T. K. Berntsen, O. Godal, R. Sausen, K. P. Shine, and T. Skodvin (2003), Metrics of climate change: Assessing radiative forcing and emission indices, *Clim. Change*, *58*, 267–331.

Gauss, M., et al. (2003), Radiative forcing in the 21st century due to ozone changes in the troposphere and the lower stratosphere, *J. Geophys. Res.*, *108*(D9), 4292, doi:10.1029/2002JD002624.

GFDL Global Atmospheric Model Development Team (2004), The new GFDL global atmosphere and land model (AM2/LM2): Evaluation with prescribed SST simulations, *J. Clim.*, *17*, 4641–4673.

Hack, J. J. (1994), Parameterization of moist convection in the NCAR community climate model (CCM2), *J. Geophys. Res.*, *99*, 5551–5568.

Hansen, J., M. Sato, and R. Ruedy (1997), Radiative forcing and climate response, *J. Geophys. Res.*, *102*, 6831–6864.

Hansen, J., M. Sato, R. Ruedy, A. Lacis, and V. Oinas (2000), Global warming in the twenty-first century: An alternative scenario, *Proc. Natl. Acad. Sci.*, *97*, 9875–9880, doi:10.1073/pnas.170278997.

Haywood, J. M., and V. Ramaswamy (1998), Global sensitivity studies of the direct radiative forcing due to anthropogenic sulfate and black carbon aerosols, *J. Geophys. Res.*, *103*, 6043–6058.

Haywood, J. M., M. D. Schwarzkopf, and V. Ramaswamy (1998), Estimates of radiative forcing due to modeled increases in tropospheric ozone, *J. Geophys. Res.*, *103*, 16,999–17,007.

Heinsohn, R. J., and R. L. Kabel (1999), *Sources and Control of Air Pollution*, 680 pp., Prentice-Hall, Upper Saddle River, N. J.

Hirsch, A. I., J. W. Munger, D. J. Jacob, L. W. Horowitz, and A. H. Goldstein (1996), Seasonal variation of the ozone production efficiency per unit NO_x at Harvard Forest, Massachusetts, *J. Geophys. Res.*, *101*, 12,659–12,666.

Holloway, T., A. Fiore, and M. G. Hastings (2003), Intercontinental transport of air pollution: Will emerging science lead to a new hemispheric treaty?, *Environ. Sci. Technol*, *37*, 4535–4542.

Horowitz, L. J., et al. (2003), A global simulation of tropospheric ozone and related tracers: description and evaluation of MOZART, version 2, *J. Geophys. Res.*, *108*(D24), 4784, doi:10.1029/2002JD002853.

Intergovernmental Panel on Climate Change (IPCC) (1990), *Climate Change 1990: The Intergovernmental Panel on Climate Change Scientific Assessment*, edited by J. T. Houghton et al., Cambridge Univ. Press, New York.

IPCC (1995), *Climate Change 1994: Radiative Forcing of Climate Change and an Evaluation of the IPCC IS92 Emission Scenarios*, edited by J. T. Houghton et al., Cambridge Univ. Press, New York.

Jacob, D. J., L. W. Horowitz, J. W. Munger, B. G. Heikes, R. R. Dickerson, R. S. Artz, and W. C. Keene (1995), Seasonal transition from NOx- to hydrocarbon-limited conditions for ozone production over the eastern United States in September, *J. Geophys. Res.*, *100*, 9315–9324.

Joshi, M., K. Shine, M. Ponater, N. Stuber, R. Sausen, and L. Li (2003), A comparison of climate response of different radiative forcings in three general circulation models: Towards an improved metric climate change, *Clim Dyn.*, *20*, 843–854.

Kheshgi, H. S., A. K. Jain, V. R. Kotamarthi, and D. J. Wuebbles (1999), Future atmospheric methane concentrations in the context of the stabili-

zation of greenhouse gas concentrations, *J. Geophys. Res.*, *104*, 19,183–19,190.

Kunhikrishnan, T., and M. G. Lawrence (2004), Sensitivity of NO_x over the Indian Ocean to emissions from the surrounding continents and nonlinearities in atmospheric chemistry response, *Geophys. Res. Lett.*, *31*, L15109, doi:10.1029/2004GL020210.

Lacis, A. A., D. J. Wuebbles, and J. A. Logan (1990), Radiative forcing of climate by changes in the vertical distribution of ozone, *J. Geophys. Res.*, *95*, 9971–9981.

Lin, S.-J., and R. B. Rood (1996), Multidimensional flux-form semi-Lagrangian transport schemes, *Mon. Weather Rev.*, *124*, 2046–2070.

Lin, X., M. Trainer, and S. C. Liu (1988), On the non-linearity of the troposheric ozone production, *J. Geophys. Res.*, *93*, 15,879–15,888.

Logan, J. A. (1999), An analysis of ozonesonde data for the troposphere: Recommendations for testing 3-D models and development of a gridded climatology for tropospheric ozone, *J. Geophys. Res.*, *104*, 16,115–16,149.

Mayer, M., C. Wang, M. Webster, and R. G. Prinn (2000), Linking local air pollution to global chemistry and climate, *J. Geophys. Res.*, *105*, 22,869–22,896.

Mickley, L. J., P. P. Murti, D. J. Jacob, J. A. Logan, D. M. Koch, and D. Rind (1999), Radiative forcing from tropospheric ozone calculated with a unified chemistry-climate model, *J. Geophys. Res.*, *104*, 30,153–30,172.

Olivier, J. G. J., A. F. Bouwman, C. W. M. v. d. Maas, J. J. M. Berdowski, C. Veldt, J. P. J. Bloos, A. J. H. Visschedijk, P. Y. J. Zandveld, and J. L. Haverlag (1996), Description of EDGAR version 2.0: A set of global emission inventories of greenhouse gases and ozone-depleting substances for all anthropogenic and most natural sources on a per country bases and on a 1 × 1 degree grid, Natl. Inst. of Public Health, Bilthoven, Netherlands.

Prather, M. J. (1994), Lifetimes and eigenstates in atmospheric chemistry, *Geophys. Res. Lett.*, *21*, 801–804.

Prather, M. J. (1996), Timescales in atmospheric chemistry: Theory, GWPs for CH4 and CO, and runaway growth, *Geophys. Res. Lett.*, *23*, 2597–2600.

Prather, M., et al. (2001), Atmospheric chemistry and greenhouse gases, in *Climate Change 2001: The Scientific Basis*, edited by J. T. Houghton et al., pp. 239–287, Cambridge Univ. Press, New York.

Ramaswamy, V., et al. (2001), Radiative forcing of climate change, in *Climate Change 2001: The Scientific Basis*, edited by J. T. Houghton et al., pp. 349–416, Cambridge Univ. Press, New York.

Randel, W. J., F. Wu, J. M. Russell III, A. Roche, and J. Waters (1998), Seasonal cycles and QBO variations in stratospheric CH_4 and H_2O observed in UARS HALOE data, *J. Atmos. Sci.*, *55*, 163–185.

Rasch, P. J., N. Mahowald, and B. Eaton (1997), Representations of transport, convection, and the hydrologic cycle in chemical transport models: Implications for the modeling of short-lived and soluble species, *J. Geophys. Res.*, *102*, 28,127–28,138.

Rasch, P., D. Zurovac-Jevtic, K. Emanuel, and M. Lawrence (2003), Consistent representation of convective processes for chemistry and climate models, *Geophys. Res. Abstr.*, *5*, 12440.

Rypdal, K., T. Berntsen, J. S. Fuglestvedt, K. Aunan, A. Torvanger, F. Stordal, J. M. Pacyna, and L. P. Nygaard (2005), Tropospheric ozone and aerosols in climate agreements: Scientific and political challenges, *Environ. Sci. Policy*, *8*, 29–43.

Schimel, D., et al. (1996), Radiative forcing of climate change, in *Climate Change 1995: The Science of Climate Change*, edited by J. T. Houghton et al., pp. 65–137, Cambridge Univ. Press, New York.

Schwarzkopf, M. D., and V. Ramaswamy (1999), Radiative effects of CH_4, N_2O, halocarbons and the foreign-broadened H_2O continuum: A GCM experiment, *J. Geophys. Res.*, *104*, 9467–9488.

Swart, R., M. Amann, and F. Raes (2004), A good climate for clean air: linkages between climate change and air pollution, *Clim. Change*, *66*, 263–269.

Wang, W. C., J. P. Pinto, and Y. L. Yung (1980), Climatic effects due to halogenated compounds in the Earth's atmosphere, *J. Atmos. Sci.*, *37*, 333–338.

Wang, W.-C., Y. Z. Zhuang, and R. D. Bojkov (1993), Climatic implications of observed changes in ozone vertical distribution in the middle and high latitudes of the Northern Hemisphere, *Geophys. Res. Lett.*, *20*, 1567–1570.

Wigley, T. M. L., S. J. Smith, and M. J. Prather (2002), Radiative forcing due to reactive gas emissions, *J. Clim.*, *15*, 2690–2696.

Wild, O., and H. Akimoto (2001), Intercontinental transport of ozone and its precursors in a three-dimensional global CTM, *J. Geophys. Res.*, *106*, 27,729–27,744.

Wild, O., and M. J. Prather (2000), Excitation of the primary tropospheric chemical mode in a global three-dimensional model, *J. Geophys. Res.*, *105*, 24,647–24,660.

Wild, O., M. J. Prather, and H. Akimoto (2001), Indirect long-term global radiative cooling from NO_x emissions, *Geophys. Res. Lett.*, *28*, 1719–1722.

Zhang, G. J., and N. A. McFarlane (1995), Sensitivity of climate simulations to the parameterization of cumulus convection in the Canadian climate centre general circulation model, *Atmos. Ocean*, *33*, 407–446.

L. Horowitz, V. Ramaswamy, and M. D. Schwarzkopf, Geophysical Fluid Dynamics Laboratory, NOAA, Princeton, NJ 08544, USA.

D. Mauzerall, V. Naik, and M. Oppenheimer, Woodrow Wilson School of Public and International Affairs, Princeton University, Princeton, NJ 08544, USA. (vnaik@princeton.edu)

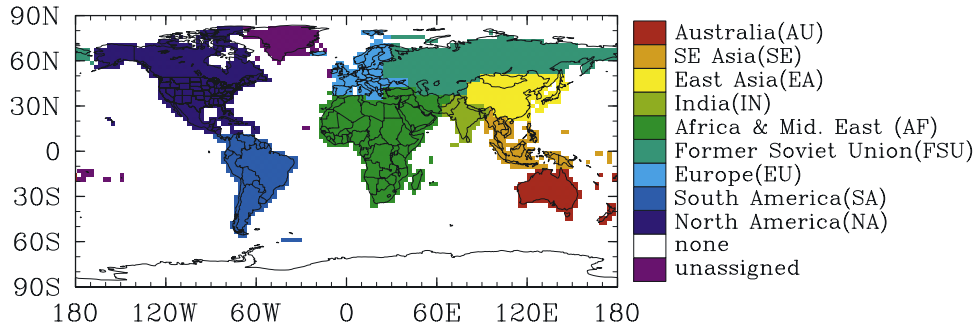

Figure 1. Map of the world showing nine regions where anthropogenic NO_x emissions are reduced by 10% for this study.

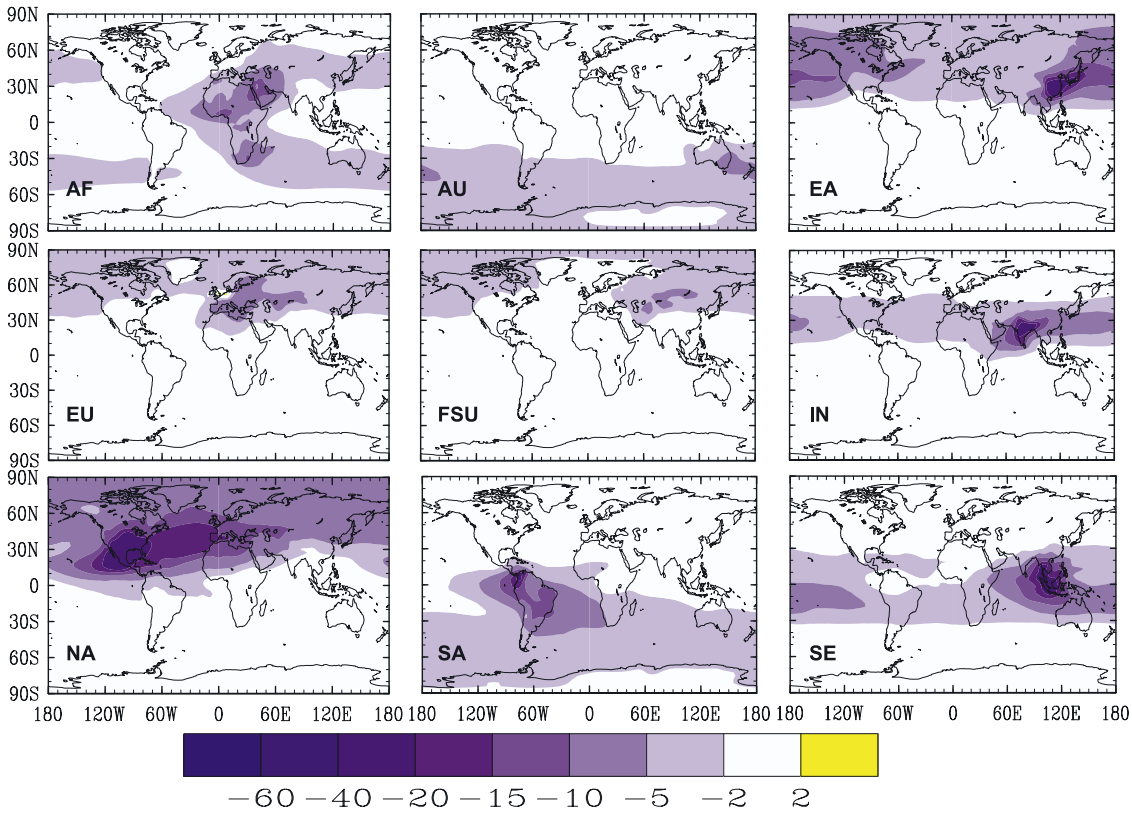

Figure 3. Simulated changes in annual column tropospheric O_3 (10^{-2} DU) due to a 10% reduction in surface anthropogenic NO_x emissions from each of the nine regions.

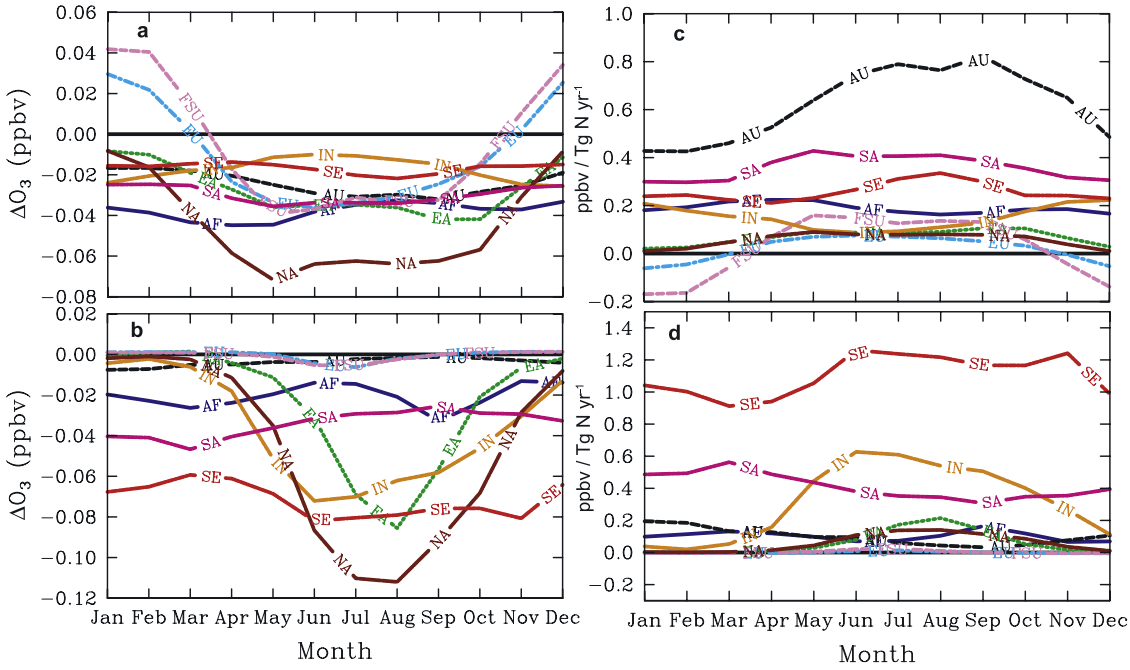

Figure 5. Monthly variation in global O_3 perturbations at (a) surface and (b) 12 km and normalized global O_3 perturbations ($\Delta O_3/\Delta E_{NO_x}$) at (c) surface and (d) 12 km, due to a 10% reduction in surface anthropogenic NO_x emissions from each of the nine regions.

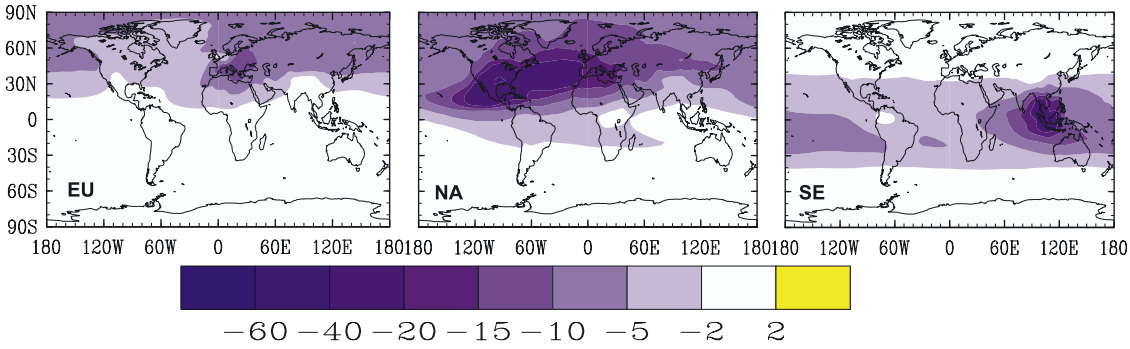

Figure 6. Simulated changes in annual column tropospheric O_3 (10^{-2} DU) due to a combined 10% reduction in surface anthropogenic NO_x, CO, and NMHC emissions from three regions.

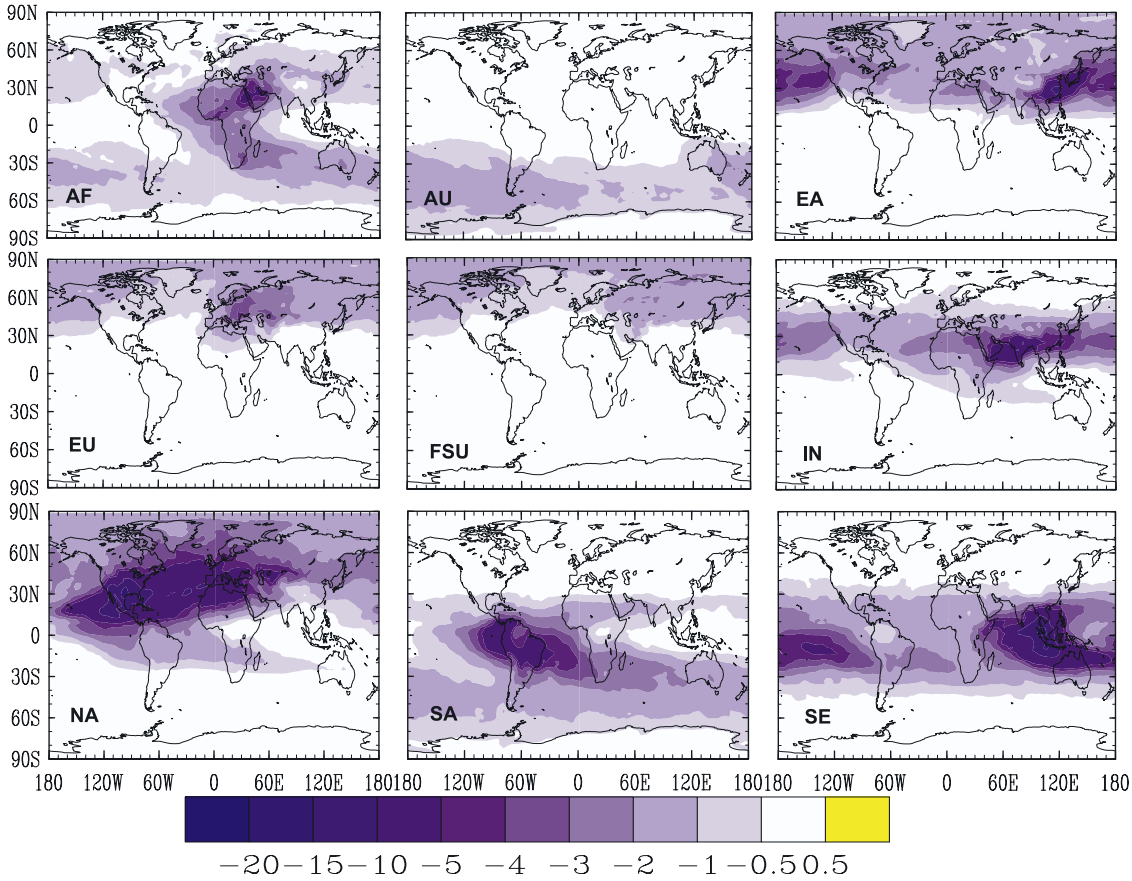

Figure 7. Annual total-sky instantaneous radiative forcing at the tropopause due to short-lived O_3 perturbations resulting from a 10% reduction in surface anthropogenic NO_x emissions from each of the nine regions.

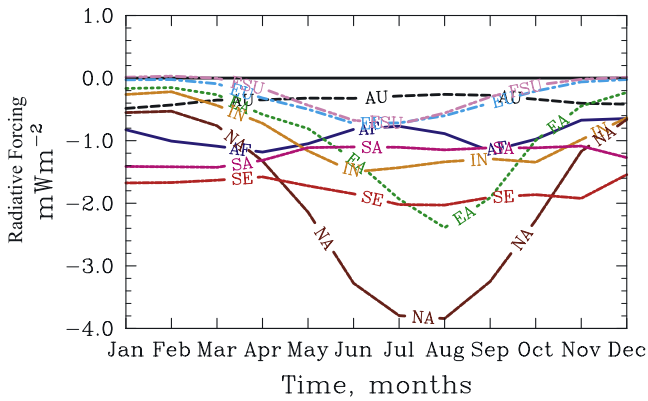

Figure 8. Monthly variation in global instantaneous radiative forcing due to short-lived O_3 perturbations resulting from 10% reduction in surface anthropogenic NO_x emissions from each of the nine regions.